Elkalashy, Nagy I.; Eldeeb, Hazem K.; Kawady, Tamer A.; Tarhuni, Naser G.; Lehtonen, Matti; Taalab, Abdel-Maksoud I.; Elsadd, Mahmoud A.

Earth fault distance estimation using travelling waves provided with triacs-based reclosing in distribution networks

Published in:
IET Renewable Power Generation

DOI:
10.1049/rpg2.12004

Published: 12/01/2021

Document Version
Publisher's PDF, also known as Version of record

Received: 12 December 2019 | Revised: 29 July 2020 | Accepted: 16 September 2020
DOI: 10.1049/rpg2.12004

IET Renewable Power Generation
The Institution of Engineering and Technology WILEY

ORIGINAL RESEARCH PAPER

Earth fault distance estimation using travelling waves provided with triacs-based reclosing in distribution networks

Nagy I. Elkalashy[1] | Hazem K. Eldeeb[1] | Tamer A. Kawady[1,2] | Naser G. Tarhuni[3] | Matti Lehtonen[4] | Abdel-Maksoud I. Taalab[1] | Mahmoud A. Elsadd[1]

[1] Electrical Engineering Department, Menoufia University, Shebin Elkom 32511, Egypt

[2] Electrical Engineering Department, Umm Al-Qura University, Saudi Arabia

[3] Department of Electrical and Computer Engineering, Sultan Qaboos University, Oman

[4] Electrical Engineering Department, Aalto University, Espoo, Finland

Correspondence
Mahmoud A. Elsadd, Electrical Engineering Department, Menoufia University, 32511 Shebin Elkom, Egypt.
Email: mahmoud.elsadd@sh-eng.menofia.edu.eg

Abstract

This study presents an earth fault distance determination algorithm for distribution networks using active travelling waves. Three triacs are used in parallel with a three-phase breaker poles to overcome the mechanical inequality of the poles' reclosing times, so that the three phases are simultaneously reclosed. As the proposed fault location technique is an active type with controllable reclosing instant, the arrival time of the reflected surge from the fault point should be stamped precisely. For this purpose, three different travelling-wave detection algorithms are evaluated including the discrete wavelet transform, Hilbert transform, and signal derivative. The fault location performance is evaluated under different fault conditions such as fault distances, fault resistances, and busbar faults. Due to utilising the reclosing transients, the proposed fault location function successfully estimates the fault distance for different earthing concepts such as unearthed, compensated, and earthed networks. This study is accomplished via simulating a typical 20 kV distribution network by the ATP/EMTP program. The results ensure the superior performance of the proposed fault distance estimation algorithm for earth faults in distribution networks.

1 | INTRODUCTION

Distribution networks are the main parts for delivering power to consumers. To improve the service continuity, most of these networks are unearthed or compensated. Earth faults occur commonly in distribution networks, where the existing massive laterals and restrictions of using widely distributed measurements complicate fault location tasks. More complexities arise in compensated and unearthed networks due to their small earth fault currents. Different concepts were introduced in the literature based on investigating either the fault impact on the fundamental components or the generated initial transients [1–4].

Fault location methods are broadly divided into three major categories including impedance, artificial intelligence, and travelling wave methods [1]. The impedance method is usually applied as the easiest one for implementation. However, the fault resistance, laterals, and loads might remarkably reduce its accuracy in distribution networks. It also depended on the feeder parameters and configuration [5, 6].

Traveling-waves method is based on the principle that the fault distance is directly proportional to the propagation time of the travelling surge between the measuring and fault points. It is expected to show excellent performance, if its challenges are overcome. The travelling-wave fault distance estimation can be a single-ended or a double-ended measurement method [7–14]. Travelling-wave fault locators are classified into passive and active ones with different modes of operation. In the passive mode, the travelling waves are created by the fault event and the reflection from the fault object are monitored and extracted to locate the fault point. Active mode is practically implemented with injecting a surge into the faulted feeder and then measuring the time instant of the reflected surge from the fault point to estimate the fault distance.

In [11–14], a promising performance of passive travelling-wave fault locations was observed depending on the aerial and ground modes. In [13], algorithms for hybrid multi-terminal networks were proposed. Compensation of the asynchronisation error was introduced in [14] as well. However, double-end measurements are required for such techniques. In [15], an active fault location method was introduced based on the difference between the created two zero-mode waves by injecting a high voltage pulse into the faulted and healthy phases separately. In [16], an active method was proposed using the travelling surges generated by switching the neutral point of the distribution transformer with a primary thyristor. However, this switching application for creating travelling waves is only restricted to unearthed and compensated networks. Other active methods were introduced by analysing the transients generated by re-energising the circuit breaker of the faulted feeder. They were based on analysing the reflected travelling surges from the fault point to the measuring point (MP) at the breaker passing through the feeder taps. However, the breaker poles are closed non-simultaneously producing different transients according to different reclosing pole instants. This represents a challenge to find the reflected surge from the fault point, precisely.

Generally, the fault location estimation methods using single-end measurements are technically preferred in distribution networks. In such networks, a serious challenge arises due to the wave reflections and refractions from the laterals and branching points. Hence, identifying the secondary waves reflected from the fault point in the complicated transient wave propagation process is difficult [17]. To identify the reflection from the fault or tapping point, transients must be extracted and decomposed. To overcome this challenge, the 'time tree' analysis of the extracted transient signals was utilised by comparing the relative distance of each peak in the signals to the known reflection points [18]. In [19], the closure-normal and reclosure-fault travelling waves of the feeder were recorded in case of normal and faulted operations, respectively. Then, the difference between these travelling-waves results in the reclosure-generated fault travelling waves reflected from the fault point with elimination of the branch and junction points' reflections. For the inaccurate control of the breaker reclosing angle, the surge amplitudes of the healthy and faulted networks are random. Therefore, the resultant travelling-wave difference may not be zeros leading to an error in estimating the fault location. Also, it lost the essence of practicality owing to be a specific algorithm to a determined network configuration.

There is no doubt that realising a travelling-wave method being unaffected by the network laterals is aimed, continually. However, different challenges arise toward this target. First, the time mismatches of the mechanical reclosing of the three-phase poles in the created travelling waves by conventional circuit breakers is a severe error source [20]. The complex topology of distribution networks with multiple laterals, busbars, parallel feeders and loads result in a conflict in identifying the reflected surge from the fault point. Also, using either earthed or unearthed distribution concepts in modern networks requires more efficient fault location tools. As example, the resulted microgrids from islanding events may be unearthed, whereas the main distribution network is still earthed. This imposes the need to a fault location method suitable to earthed and unearthed distribution networks. Moreover, the nature of the distribution network operation suffers from sustained changing of the network topology. This may lead to restrictions on the use of the results obtained from the pre-transient data for fault location purposes. On the other hand, the gradual attenuation of the reflected surges from the fault point forces to depend on the first arrival of the reflected surge. Hence, obtaining the time stamping of the arrival surge from the fault point accurately is necessary even under high impedance earth faults.

In this paper, a novel active fault-locator algorithm is presented. The presented algorithm is suitable for both earthed and unearthed distribution networks. The earth fault distance is calculated by obtaining the instant of the first arrival surge of zero-mode voltage to avoid the gradual attenuation of the reflected surges. The first arrival surge of zero mode at the MP is certainly reflected from the earth fault point whatever the distribution network topology (parallel feeders, laterals, etc.) under the condition of simultaneous reclosing for the controlled triacs parallel with the circuit breaker poles. This simultaneous reclosing leads to that the first arrival surge of zero mode is a reflected phase-surge from the earth fault point (the propagation speed of the arrival surge equals that of faulted phase) and its arrival time is proportional to the earth fault distance. Also, the time stamping of this first arrival surge is obtained utilising the signal derivative approach based on a new adaptive thresholding procedure. The new adaptive procedure enhances the accuracy of the fault location estimation under earth faults associated with high fault resistance. The study is organised in such that the proposed fault-locator algorithm is explained in Section 2. Then, the selected simulation system is introduced in Section 3. Performance evaluation tests are investigated in Section 4. Practical issues of the proposed fault locator are discussed in Section 5. Performance comparisons with other travelling-waves methods are accomplished in Section 6 The study conclusions are finally summarized in Section 7.

2 | THE PROPOSED FAULT-LOCATOR ALGORITHM

2.1 | Triac-based simultaneous reclosing mechanism

The flowchart of the proposed fault-location method is depicted in Figure 1. Once an earth fault was detected, the circuit breaker disconnected the faulted feeder down. Then, the three-phase triacs are simultaneously reclosed at the peak voltage instant of the faulted phase through a dedicated peak voltage detector. From the travelling point of view, the incident v_{i-a} magnitude is intently increased by reclosing the triacs at the peak voltage instant of the faulted phase. This ensures realising the most possible high travelling-wave surge for a reliable and precise computation of the fault location. This simultaneous reclosing of the three phases resulted in having no zero-mode travelling waves along the healthy parts of the feeder including the tapping points as derived above. This completely avoids wave reflection from the healthy tapping points. The fault point can only reflect the travelling wave through the faulted phase in the zero mode toward the MP through the RC

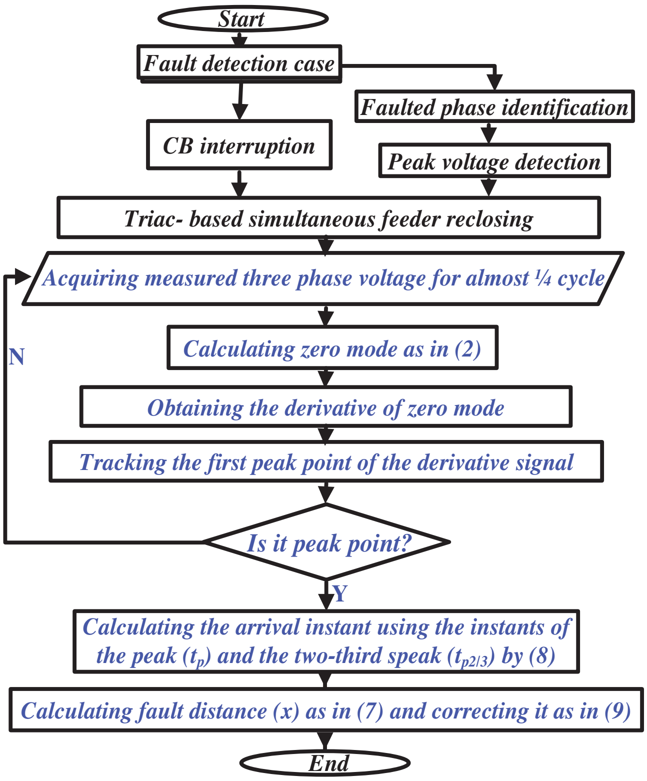

FIGURE 1 The flowchart of the proposed method

(resistor-capacitor) transducer at the main busbar. Accordingly, the first received travelling wave can be certainly utilised for locating the fault point effectively.

2.2 | Fault location computational basis

The proposed earth fault-locator algorithm precisely obtains the fault distance by utilising the first arrival of reflected waves from the fault and cancelling the reflected signals from lateral points. Moreover, it is sensitive to high impedance earth faults depending on an accurate time stamping method of the first arrival surge. The proposed algorithm is based on monitoring the zero-mode voltage at the MP through the RC transducer at the main busbar as shown in Figure 1. The first arrival surge of zero mode is reflected from fault point. This is verified using simultaneous reclosing for the three phases at a certain time by the utilised triacs.

By assuming that the utilised triacs are simultaneously reclosed at a time instant t_0, the incident three-phase voltages (v_{i-a}, v_{i-b}, and v_{i-c}) at the simultaneous reclosing instant of the three poles are written as

$$\begin{cases} v_{i-a} = V_p \cos(\omega t_0) \\ v_{i-b} = V_p \cos\left(\omega t_0 - \frac{2}{3}\right) \\ v_{i-c} = V_p \cos\left(\omega t_0 + \frac{2}{3}\right) \end{cases} \tag{1}$$

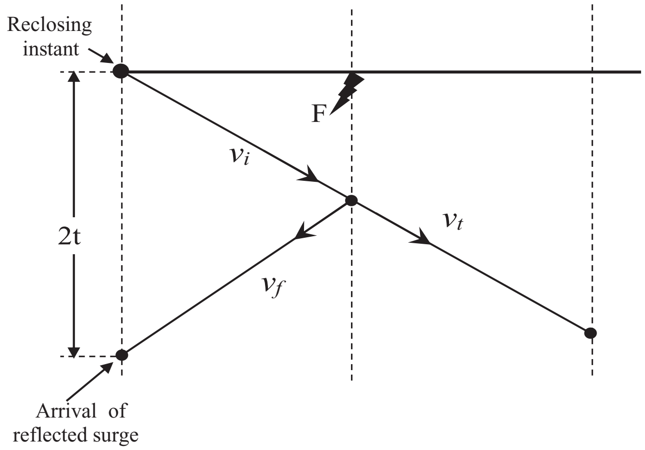

FIGURE 2 Three-phase voltage lattice diagram. The incident voltage $v_i = [v_{i-a}\ v_{i-b}\ v_{i-c}]^T$, the reflected voltage $v_f = [v_{f-a}\ v_{f-b}\ v_{f-c}]^T$, and the transmitted voltage $v_t = [v_{t-a}\ v_{t-b}\ v_{t-c}]^T$

where, V_p is the peak voltage, and ω is the angular velocity. Then, the incident wave zero mode v_{i-0} voltage is attained as

$$v_{i-0} = \frac{1}{3}\left(v_{i-a} + v_{i-b} + v_{i-c}\right) \tag{2}$$

From Equations (1) and (2), the travelling wave zero-mode voltage is equal to zero due to balanced incident voltages v_{i-a}, v_{i-b}, and v_{i-c}.

$$v_{i-0} = 0 \tag{3}$$

However, the travelling surges in the three phases propagate separately. Although there are reflections at the lateral points, their summation is still equal to zero. The reached surge to the fault point is then reflected and a non-zero summation value is ascertained. Then, the surge reflected from the fault point is returned backward to the measuring point as illustrated in Figure 2. Fortunately, this reflection from the fault point is significantly visible in the wave zero-mode component at the measuring point. To derive this information, a lossless line modeling is assumed, and then the reflected surge (v_f) at the fault point of each phase is [15],

$$v_f = \left[v_{f-a} \quad v_{f-b} \quad v_{f-c}\right]^T \tag{4}$$

$$v_f = -\frac{v_i - \alpha}{Z_s + 2R_f}\left[Z_s \quad Z_m \quad Z_s\right]^T \tag{5}$$

where v_{f-a}, v_{f-b}, and v_{f-c} are the reflected surges over the phases a, b, and c, respectively. Z_m is the wave mutual-impedance, R_f is the fault resistance, and Z_s is the wave self-impedance as defined in [15]. Then, the first arrival zero-sequence mode of the reflected surge is

$$v_{f-0} = -\frac{v_{i-a}}{Z_s + 2R_f}\left(Z_s + 2Z_m\right) \tag{6}$$

Based on Equation (6), the incident voltage of the faulted phase (v_{i-a}) mainly contributes to the reflected wave zero mode. As the zero-mode voltage in Equation (6) only contains the faulted phase voltage, the propagation speed value of this phase is used to compute the fault distance. The fault distance (d_e) is calculated by assuming that both the utilised triacs are simultaneously reclosed at a time instant t_0 and the created travelling waves propagated toward the fault point and then reflected from the fault point discontinuity to the measuring point at a time instant t_1 as

$$\left.\begin{aligned} d_e &= c \times t \\ t &= (t_1 - t_0)/2 \end{aligned}\right\} \tag{7}$$

where t is the propagation time from the triacs to the fault and return to the measuring point. The value c is the travelling wave propagation speed. Based on feeder parameters estimated by the LCC model of the feeder built-in of the ATP program, the utilised propagation speed of the phase voltage is 294 km/ms. This value is confirmed by comparing the travelling surge of the phase voltage and the zero-mode voltage applied with reclosing transients, where their arrivals are identical. Then, 294 km/ms is the correct speed to estimate the fault distance using the proposed triacs-based reclosing.

2.3 | Travelling wave surge extraction using adaptive threshold- based signal derivative procedure

One of the main challenges of travelling-waves fault locators is to precisely stamp the surge arrival times of the reflected signal from the fault point. Since the instant of triggering of the three-phase triacs is well-known, the precise measuring of the first arrival surge leads to realising the aimed performance of the proposed fault-locator algorithm. For this target, three well-known surge extraction methods were tested as a digital processing tool to extract the reflected surges including discrete wavelet transform (DWT), Hilbert transform, and signal derivative. These methods were thoroughly investigated to pinpoint the most suitable extraction method. Owing to these tests, the signal derivative method was verified for identifying the first surge, correctly. This method is simple and reliable for extracting the time stamping of the arrival surge [16]. Also, a new adaptive thresholding procedure is suggested considering both the time stamping and the amplitude of the first peak of the derivative signal. The root of the reflected surge arrival time (t_1) is calculated based on the instants of the peak (t_p) and the two-thirds peak ($t_{p2/3}$) of the derivative as

$$t_1 = t_p - 3\left(t_p - t_{p2/3}\right) \tag{8}$$

The numerical coefficient of the value of 3 in Equation (8) is logically used to return back from the peak instant t_p, where this return is three times of the time difference between the peak instant and the two-thirds peak instant (t_p–$t_{p2/3}$). The fault distance d_e is estimated using Equation (7), while it is based on an adaptive threshold value as investigated in Section 4.

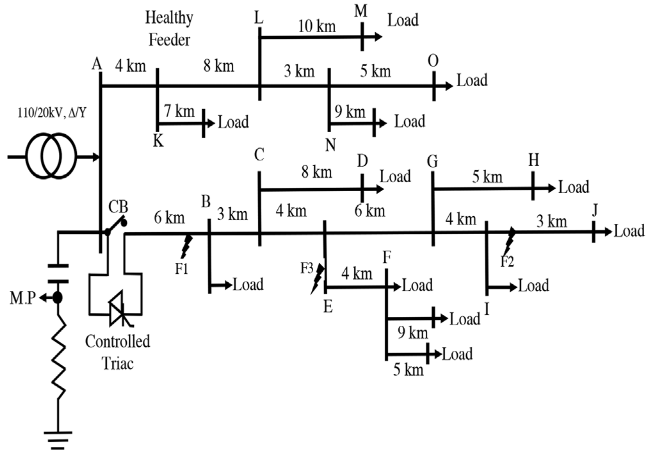

FIGURE 3 A single line diagram of a typical 20 kV feeder illustrating both the inserted triac location and the measuring point (MP)

3 | SELECTED SIMULATION SYSTEM

Figure 3 shows the single line diagram of the selected 20 kV unearthed overhead distribution line with two feeders, multiple loads, and sublaterals. It was simulated using the ATP/EMTP program for investigation purposes, where the ATPDraw was used for pre-processing computation. Furthermore, other earthing concepts is considered in Section 6 to evaluate and confirm the applicability and the universality of the proposed fault location algorithm. The RC transducer branch is used to monitor the voltage travelling waves with a sampling rate of 10 MHz. For high voltage networks, the capacitor dividers were typically utilised for capturing surges as seen in [21, 22]. Either the considered RC branch or a conventional current transformer is suitable, however, the RC branch was utilised for capturing the travelling waves in this study. That is because there are no current transients at the beginning of the faulted feeder, if the distribution network in Figure 3 is a single-feeder (the faulted feeder only). In this case, the feeder at the measuring point can be represented as an open circuit terminal for the travelling waves. Accordingly, the voltage transients are considered. With the utilised RC transducer, the capacitor was used for isolation and voltage reduction purposes. The resistor was used to capture the derivative of voltage waveform that enhances the captured transients rather than the fundamental voltage. As in [16], a capacitor of 0.01 μF and resistor of 100 Ω were selected, in which they produce a measuring signal with a ratio of $R \times C = 10^{-6}$ of the voltage waveform derivatives. As derived in Section 2, the zero-mode formula is appropriate to pinpoint the faulted phase discontinuity.

Three fault positions were considered in the distribution system shown in Figure 1 for evaluating the proposed fault location algorithm. Line faults are considered at F1 at 5 km in section AB and F2 at 24 km in Section 2. Busbar faults are represented by

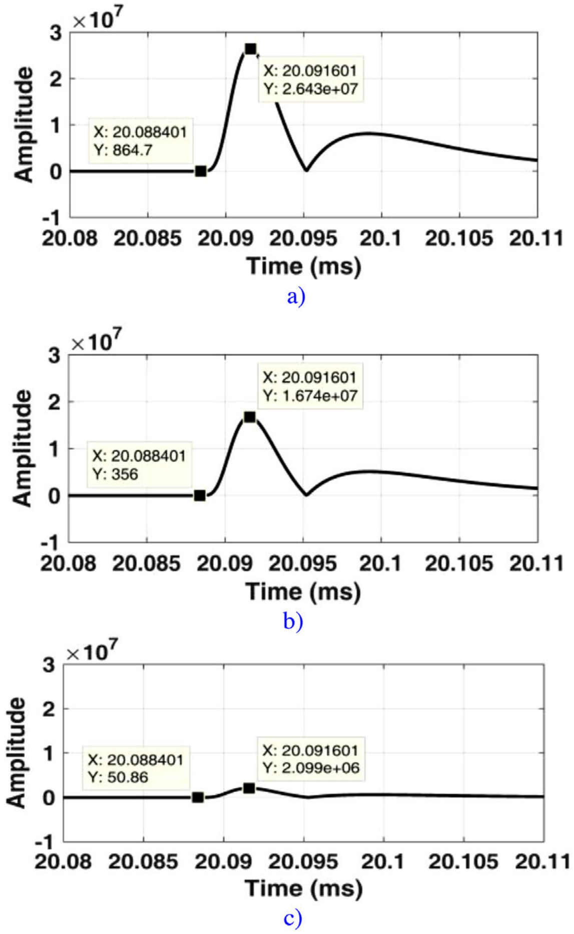

FIGURE 4 Output of signal derivative (reclosing instant at 20 ms) under fault F3 associated with different fault resistances that are (a) 0.01 Ω, (b) 100 Ω, and (c) 2 kΩ

another fault point F3 at 13 km at busbar E. These distances are considered with reference to the measuring point at the main busbar A. To locate a fault of these considered fault points, the proposed scenario of triacs-based simultaneous three-pole reclosing is accomplished and then the travelling-wave surge is extracted using the adaptive threshold procedure.

4 | PERFORMANCE EVALUATION TESTS

4.1 | Computational core performance

Depending on the selected 20 kV test system, the signal derivative method based on the adaptive threshold procedure is investigated. Due to that, the instant of triggering the triacs is well-known; the precise measuring to the first arrival surge leads to realising the aimed performance of the proposed fault-locator algorithm. Based on the zero-mode voltage signal, the exact time stamping for fault F3 under different fault resistances up to 2 kΩ is shown in Figure 4. Figure 4 shows both the significant reduction of the peak of the derivative signal and the

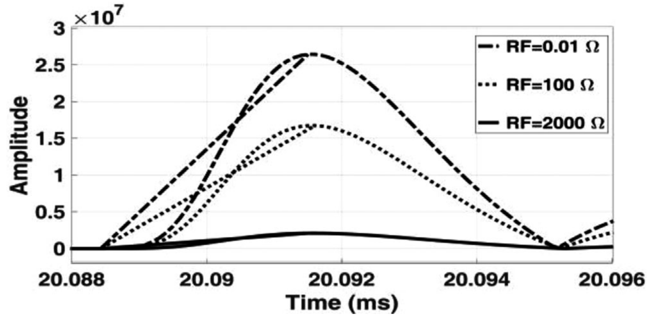

FIGURE 5 Output of signal derivative under fault F3 focusing on the region between the peak and the actual arrival surge instant

slight change of the derivative signal amplitude at the actual time stamping with fault F3 under changing the fault resistance. Therefore, utilising a fixed threshold value leads to errors in extracting the arrival instant despite the slight change.

To increase the accuracy of extracting the time stamping, the presented adaptive thresholding procedure is utilised. The root of the reflected surge arrival time (t_1) is obtained utilising both the peak instant and the two-thirds peak instant as in Equation (8) based on obtaining the first peak amplitude of the derivative signal. This is explained by focusing on the region between the peak and root of the reflected surge arrival time as in Figure 5 under fault F3. The proposed formula of Equation (8) is obtained by plotting a straight line between the peak point and the derivative signal amplitude at the actual time stamping as in Figure 5. Fortunately, the intersection of this straight line and the derivative signal is almost at two-thirds peak value whatever the fault resistance value as shown in Figure 5. Thus, the time stamping is accurately obtained using the known formula of the straight line. The obtained time stamping under fault F3 (13 km) associated with solid, 100, and 2000 Ω is almost 0.0882 s indicating to an estimated fault distance (d_e) that almost equals 12.97 km as shown in Table 1.

Fault F3 is chosen where it is in the middle of the tested feeder. Under faults upstream fault F3 (i.e. fault F1) the intersection point take places at a point less than two-thirds peak value and vice versa. Therefore, the estimated distance (d_e) under fault F1 is less than the actual fault distance, whereas the d_e under fault F3 is more than the actual fault distance as shown in the shaded cells in Table 1. Consequently, the obtained fault distance is corrected using second-order polynomial coefficients as

$$d_{cor} = 1.0128\, d_e - 8.13 \times 10^{-4}\, d_e^{\,2} \tag{9}$$

where d_{cor} is the corrected fault distance. This formula is obtained by profiling the correlation of the estimated fault distance with the corresponding actual fault distance along the entire range of the feeder length. This equation is valid for the travelling waves transient detection, where the travelling wave concept is the same for any homogenous power network concerning the propagation and attenuations. However, the non-homogenous networks containing sections of overhead

TABLE 1 Proposed surge extraction using adaptive threshold-based signal derivative procedure

Fault case	Proposed method response						
d_f	R_f (Ω)	t_p	$t_{2/3}$	t_1	d_e	d_{corr}	ε%
5 km (section AB)	Solid	20.0347	20.3441	0.03367	4.950	4.994	–0.12
	100	20.0347	20.3441	0.03368	4.951	4.995	–0.10
	2000	20.0347	20.3441	0.03369	4.953	4.997	–0.06
13 km (busbar E)	Solid	20.0916	20.0904	0.08823	12.969	13.003	–0.06
	100	20.0916	20.0904	0.08825	12.973	13.006	–0.01
	2000	20.0916	20.0904	0.08828	12.977	13.011	0.02
24 km (section IJ)	Solid	20.1704	20.1683	0.16426	24.146	23.997	0.05
	100	20.1704	20.1683	0.16429	24.152	24.002	0.06
	2000	20.1705	20.1683	0.16417	24.134	23.984	–0.07

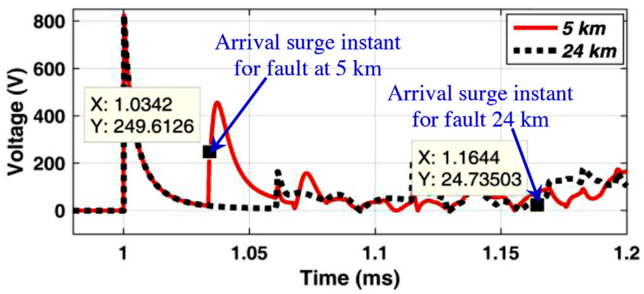

FIGURE 6 Zero-mode voltage waveforms for non-simultaneous reclosing onto fault cases F1 (5 km) and F2 (24 km)

and underground cable segments have different propagations and attenuations. This may result in different fitted coefficients for errorminimisation. Accordingly, the resulting fault location error was reduced to the range less than ± 0.1 % where the percentage error of the obtained fault distance is computed as

$$\varepsilon\% = \frac{d - d_f}{d_f} \times 100 \tag{10}$$

where d_f is the actual fault distance for each simulated fault case.

4.2 | Impacts of non-simultaneous reclosing action

In order to highlight the role of the parallel triacs for reclosing the faulted feeder, the performance of non-simultaneous reclosing poles was investigated first. As seen in [20], the three poles of the circuit breaker were non-simultaneously reclosed, where phase-a was closed first at 1 ms. After 0.63 ms, phase-b was closed. Finally, phase-c was closed after 1.1 ms from phase-a closing instant. Applying this reclosing scenario in the fault cases F1 and F2 resulted in the reflected zero-mode signals shown in Figure 6. Unfortunately, there is a zero-mode waveform at the first phase reclosing instant at 1 ms. The arrival instant in case of fault F1 could be correctly detected with the first surge (the red waveform) as the fault was in the first section AB before the tapping points. However, it is complicated to detect the arrival instant of fault F2 (dotted black waveform) because of the multiple reflections of the tapping points. These results confirmed the efficacy of the proposed simultaneous reclosing action using the triacs.

4.3 | Phase currents and voltages of proposed fault-locator algorithm scenario

Figure 7 shows the phase currents and voltages in addition to the response of the proposed algorithm for fault F1 case with the reclosing instant (t_0) at 20 ms. As illustrated in Figure 7(a), the three-phase triacs were triggered together feeding the transient currents simultaneously. This period of transient currents is sufficient to create the surges to be exploited for estimating the fault distance. Figure 7(b) shows the corresponding voltage transients. As shown in Figure 7(c), the zero-mode voltage was kept at zero until the arrival of the reflected surge from the fault point appearing at a time instant of 20.034 ms. As compared with the reclosing instant (t_0) and the surge reflection instant (t_1), the elapsed time ($2t$) was 0.034 ms. It is worth to note that the zero-sequence mode in Figure 7(b) was calculated using the system voltage waveforms, while the zero-mode voltage in Figure 7(c) was calculated using the waveforms measured via the RC transducer. As shown in Figure 7(c), the measured zero-mode voltage precisely indicates the reflection instant, since the measured signals over the RC transducer is the derivative of the voltage phase signals as illustrated and declared in [16].

Figure 8 shows the response of the proposed algorithm for the fault case F2 at 24 km insection IJ. As depicted in Figure 8(a), the fault reflection surge cannot be estimated from the reflections in phase voltage waveforms. However, the zero-mode waveform was kept zero until the arrival of the fault reflection surge at the instant of 20.1644 ms as confirmed

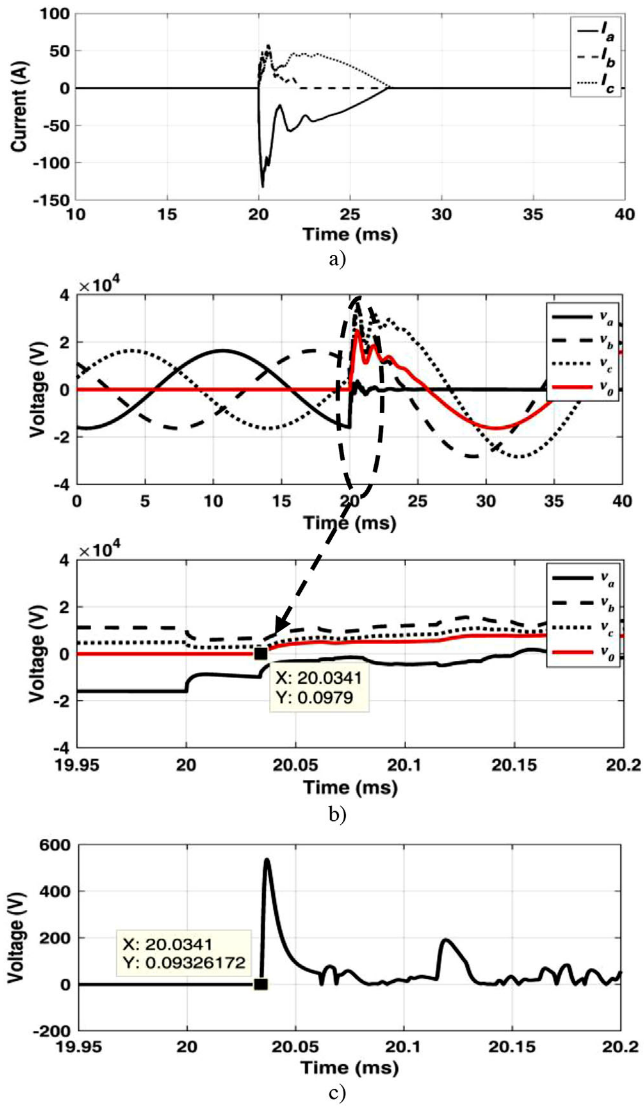

FIGURE 7 Reclosing response for ground fault F1 at 5 km in section AB showing both (a) triac currents with simultaneous reclosing, (b) three phase and round voltage transients, and (c) computed zero-mode voltage at the MP

from the measured zero-mode voltage via the adopted RC transducer as shown in Figure 8(b). These results for both fault cases corroborated the accuracy of the proposed fault distance estimation method using the created transients by triacs-based simultaneous reclosing mechanism. The simulated system shown in Figure 1 consists of two feeders, where the measuring of the reflected surge is at the common busbar. At this busbar, the network is in-service with the healthy feeder, while the triacs reclose the faulted feeder. As depicted in Figure 1, the first section AK in the healthy feeder has a length of 4 km, which is shorter than both assigned fault cases F1 (5 km) and F2 (24 km). However, Figures 7 and 8 show the reflected surge in the zero-mode voltage without any reflections from busbar K in the healthy feeder for both fault cases. This is because the zero mode has a zero value at the reclosing instant and its travelling through the healthy feeder has a zero reflection from busbars.

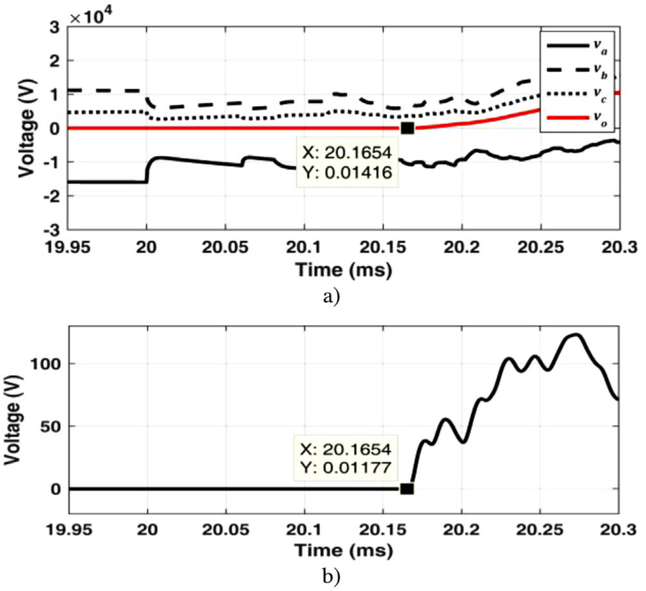

FIGURE 8 Reclosing response for fault F2 at 24 km in section IJ where (a) voltage transients and (b) v_0 waveform calculated using voltages measured over the RC branch

4.4 | Impacts of unbalanced distribution network

Unbalanced distribution networks may be due to unbalanced phase voltages of the source feeding the primary substation or due to unbalanced loads. These situations should be evaluated because the mathematical base of the proposed locator was constructed considering a balanced three-phase distribution network. Figure 9 shows the system response for an amplitude imbalance of one phase with 20% reduction of the source voltage. The reclosing instant is at 20 ms for an earth fault at F2 of the feeder (at 24 km). Although the zero-mode voltage computed at the fundamental frequency appeared in the measurements at the source side as depicted in Figure 9(a), no zero-mode voltage was remarked at the measuring point (at the main busbar of the distribution feeder). The zero-mode voltage was zero until the reflected surge was returned from the fault point as depicted in Figure 9(b). Accordingly, travelling wave reflecting from the fault point is extracted using the zero-mode voltage at the measuring point at the main distribution system busbar. This performance was attained because of the main power transformer connectivity of delta/star connection. Generally, the power transformer connection isolates the zero mode between the source side and distribution network.

In Figure 10, the performance of the proposed locator was examined with the simultaneous reclosing having different unbalanced conditions demonstrating the zero-mode voltage for the fault cases F1 and F2. First, the 20% reduction of the voltage amplitude of the phase voltage was seen in Figure 10(a), where sensing the time of the first surge arrival was still applicable and fault distance can be estimated correctly. Similarly, an unbalanced phase shift of 39.6 degrees in

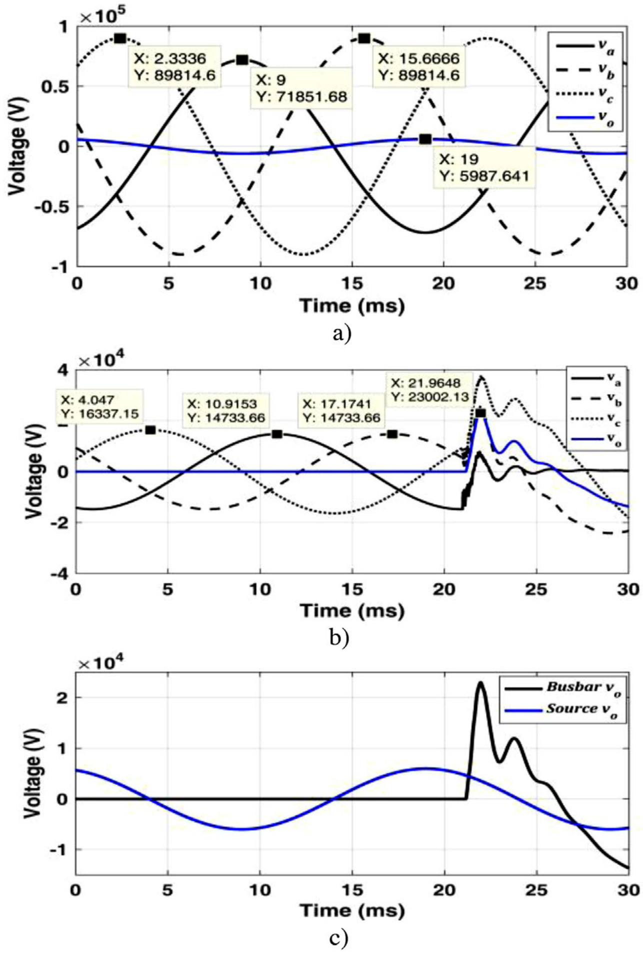

FIGURE 9 Unbalanced phase voltages of the source during the triacs-based reclosing for fault case F2 where (a) phase and zero-mode voltage waveforms measured at the source side, (b) phase and zero-mode voltage waveforms MP busbar, and (c) zero-mode voltages at the source side and main busbar

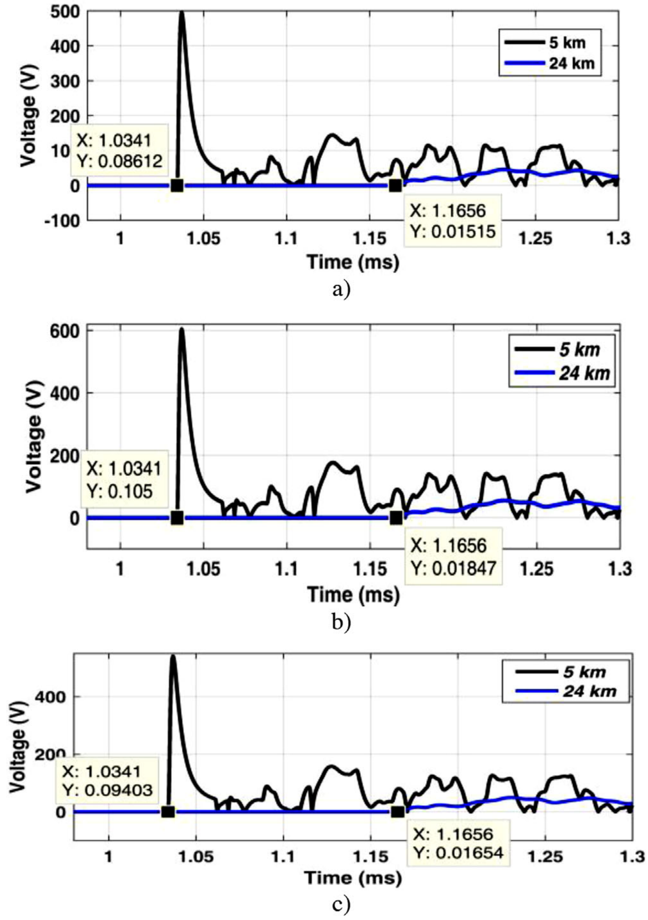

FIGURE 10 Output of zero-mode voltage under different conditions for unbalanced source voltages that are (a) amplitude unbalanced with 20% reduction in a phase voltage, (b) phase shift unbalanced with 39.6 degress in a phase angle, and (c) combined amplitude/phase unbalance

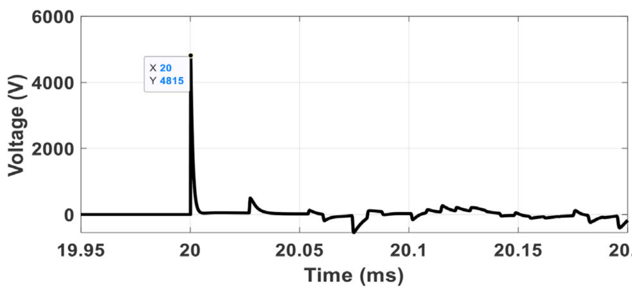

FIGURE 11 Computed zero-mode voltage at the MP for a fault just behind the triac element at the feeder side

the phase angle was examined as illustrated in Figure 10(b), whereas a case of both combined magnitude and phase angle unbalanced conditions was examined successfully as depicted in Figure 10(c). As revealed from the results, the proposed method was not affected by these unbalanced conditions in the source voltage for both close and far faults, where no zero-mode voltage was remarked at the measuring point before the reclosing instant. On the other hand, unbalanced loads do not participate as well at the reclosing instant because of the transformer winding connection, and consequently they do not impact the performance of the proposed locator.

5 | PRACTICAL ISSUES OF THE PROPOSED FAULT ALGORITHM

In order to realise an applicable protective scheme, it should be characterised with some features such as generality, ease of setting, implementation possibility, challenges and so forth. These issues are considered as discussed as follows.

5.1 | Close-in fault location

Although the travelling-wave fault location techniques is usually more accurate than other impedance-based techniques, there is a challenge to locate very close faults to the measuring busbar as there is no travelling time. It is therefore essential to investigate such situations. Figure 11 shows the computed zero-mode voltage at the measuring point for a fault just behind the triacs' terminals at the feeder side with a reclosing time instant of 20 ms.

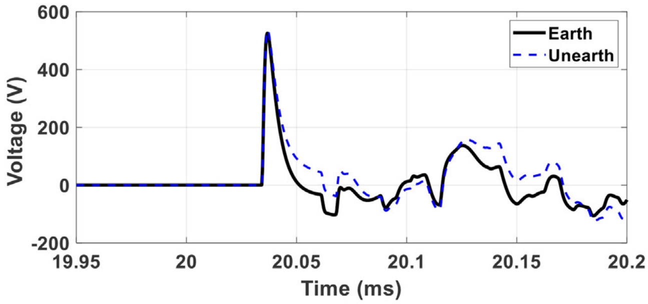

FIGURE 12 Computed zero-mode voltage at the MP for ground fault F1 at 5 km in section AB with earthed/unearthed distribution feeder

It is revealed that the computed zero-mode voltage immediately appeared at the reclosing instant (20 ms) at the measuring point estimating a zero-fault distance. As compared with the past fault cases at F1, F2 and F3, the whole line length is perfectly covered.

5.2 | System earthing concept

As mentioned earlier, unearthed distribution feeder was considered through the previously applied tests. The proposed fault location technique is advantageous depending on the active travelling waves using simultaneous reclosing transients. Accordingly, it is suitable for all earthing concepts in distribution networks. For illustration purposes, the F1 earth fault at 5 km was repeated considering solidly earthed system as depicted in Figure 12. As compared with the corresponding case with unearthed condition, the first reflected surge due to simultaneous reclosing is not affected by the earthing concept. Accordingly, the proposed fault location technique estimates the fault distance accurately whatever the earthing concept.

5.3 | System implementation

The proper detection of the reflected surge and ,consequently, a correct computed fault location depend on the selected time sampling rate. As seen in [32], 1 μs of timing error could result in a fault-locating error of around 150 and 75 for overhead and underground lines, respectively. Hence, 10 MHz was considered in this study for realising a precise estimated fault distance. It is a typical sampling rate for recent publications with travelling waves for protection applications [33]. On the other hand, the aimed fault location is computed off-line after de-energising the conducted triacs. Hence, the selected sampling rate can be implemented nowadays with modern DSPs or microcontrollers in a straightforward manner.

The travelling-wave speed of overhead lines is different than the corresponding one of underground cables. Therefore, a single travelling-wave propagation speed can be used for homogeneous feeders. However, composite feeders with both cable/line segments provide a challenge for travelling-wave fault location. This case may need more investigations such as the reported methods in [16] and [30], where the underground cable sections are converted to their equivalent overhead line distances using a specific conversion factor 1/0.55. Then, the fault distance is estimated for the overall equivalent overhead feeder using the arrived travelling surges. Finally, the cable section inversion is applied to exactly estimate the fault distance from the measuring point.

Recently, smart grids become the most important target for modern utilities based on self-healing, fault management and system restoration processes [31]. However, the reclosure action onto the faulted feeder is not allowed in the fault management procedures. Then, applying the travelling-wave fault location using transients created by breaker re-energising is not permitted in smart grids. However, the proposed algorithm has the advantage of applicability to smart grid systems because the network is not harmed by the controllable reclosing triacs with a current period less than a half of the power cycle. However, the dv/dt and di/dt capability limits for both the off-state and on-state of the utilised triacs should be selected carefully. Also, the on-state surge current should be considered for triacs applications. For the distribution feeder under study, the added triacs should withstand the instantaneous maximum current of 135 A as depicted in simulation results shown in Figure 7(a). This short period of low currents is because the triacs triggering is at the faulted phase-voltage peak instant. As the feeder is simply an inductive element, the fault current is shifted by a significant angle than the voltage. Also, the fault current is interrupted at the first coming zero-crossing through the triacs and the currents do not reach the damage levels as seen in Figure 7(a). Accordingly, the triacs carry currents less than the expected short circuit current with the voltage level of the distribution range of 20 kV. From the power network point of view, the fault transient stress is less than a half of a cycle. On the other hand, the fault detection phase consumed more than a cycle for relaying and three to five cycles for the circuit breaker interruption. Therefore, the total clearing time is between four to six cycles. Comparing the conventional fault clearing time and forced transients by the triacs reclosing action, the network withstand with the reclosing time is possible.

5.4 | Algorithm sensitivity against high impedance faults

In the studied tests, the fault resistance is considered from solid fault up to high impedance fault that it is considered within the fault resistance range from 0.01 to 2000 Ω. Therefore, the solid earth fault is represented by 0.01 Ω, whereas the earth fault current due to the 2000 Ω fault resistance in 20 kV distribution network is $(20000/\sqrt{3})/2000$ A (5.7 A). This fault current is extremely low, in which it cannot be detected using the conventional protection systems. Thus, it represents a very high impedance fault case. Evaluating the proposed algorithm under this range of the fault impedance (from solid to high impedance faults) ensures the proposed algorithm capability for accurately locating the faults for the distribution network. This fault location determination is enhanced by considering high surge amplitude as the proposed algorithm is active type and the reclosing

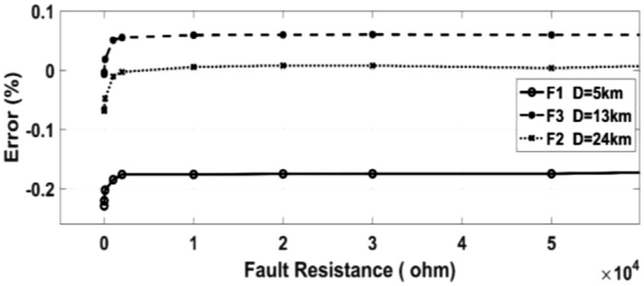

c)

FIGURE 13 Response of method [15] for the earth faults F1, F2, and F3

instant is controllable using the triacs-based reclosing system. The reclosing instant is at the peak value of the faulted phase to send the highest travelling surge supporting and then to overcome the fault resistance reflection effect.

Although the conventional protection systems could not detect high resistive faults reliably, the capability of the proposed fault-locator algorithm against faults associated with fault resistances up to 50 kΩ was verified as depicted in Figure 13. Such very high impedance fault cases can occur in real fields in some circumstances such as tree contacts or downed conductors. The same performance was also expected, if an arcing is accompanied into the fault path. Actually, those protection functions depending on travelling waves are usually less sensitive to nonlinear arcing elements as concluded in [34].

5.5 | Algorithm security against fast transients

The proposed fault location algorithm is based on active travelling surges that are created using triacs-based three-phase simultaneous reclosing of the faulted feeder. This is called active travelling waves fault location where the instant of reclosing is well-known and utilised for time difference estimation. However, touching the faulted feeder during the reclosing instant is expected with low probability. For the security point of view, the fault location determination process can be calculated several times by repeating the triacs-based reclosing action several times, for example attaining the fault distance estimation three times. This can ensure and secure the estimated fault distance.

6 | PERFORMANCE COMPARISON WITH OTHER TRAVELLING-WAVES METHODS

To generalise the performance evaluation of the proposed fault-locator algorithm, a comparative study was accomplished between the proposed algorithm and other existed travelling-waves methods in two phases. The first phase is between the proposed method and other travelling-wave methods, whereas the second one is between the used adaptive threshold value-based signal derivative procedure and other existed signal processing methods. The comparative study contains a variety of fault resistance range and fault distance.

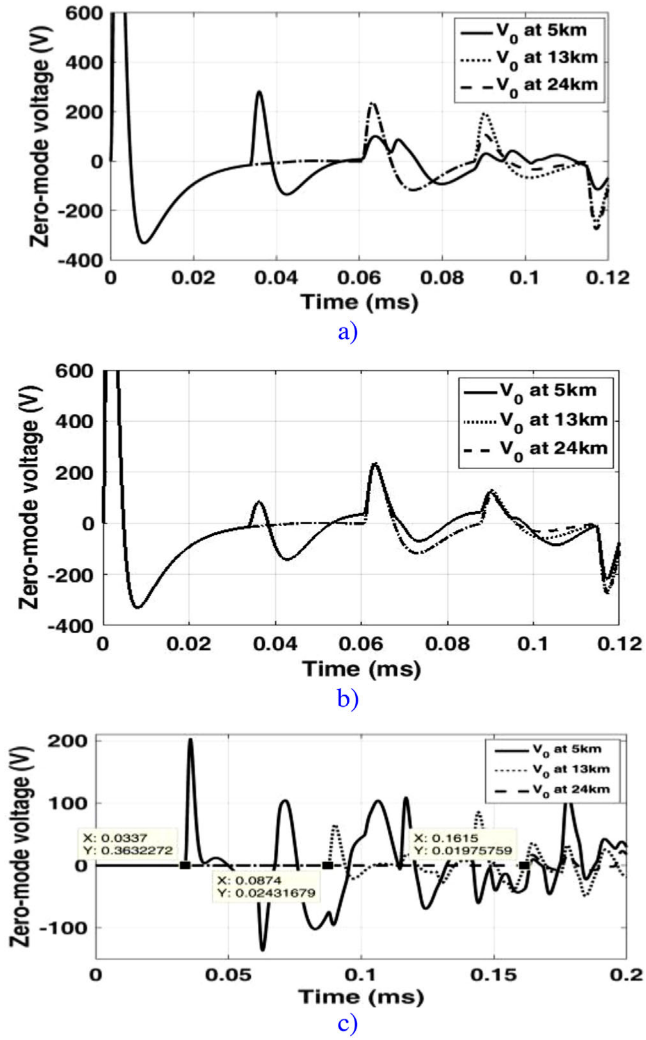

FIGURE 14 Response of [15] under different ground faults F1, F2, and F3 with unearthed distribution feeder illustrating the measured zero-mode voltage under injecting a pulse. (a) Healthy phase, (b) faulted phase, (c) difference between the two zero-mode voltages

6.1 | Comparison with fault location algorithms

In the first phase, the comparative study was accomplished with two travelling-wave fault location methods presented in both [15] and [19]. The procedure presented in [15] is implemented and tested under different fault cases. Its response is illustrated in detail in Figure 14 under three different earth fault cases F1, F2, and F3 assigned in Figure 1. Figures 14(a) and (b) show the measured zero-mode voltages under separately injecting a high voltage pulse with 10 kV amplitude on the healthy and the faulted phases, respectively. Comparing the two groups of zero-mode voltage under these two injection cases is shown in Figure 14(c), and the fault distance is obtained using the

TABLE 2 The presented method response versus other existing methods under earth faults at different conditions

		[15]		[19]		Proposed method	
Fault at (km)	R_f (Ω)	D_{EST} (km)	ε %	D_{EST} (km)	ε %	D_{EST} (km)	ε %
5 (at AB)	Solid	5.055	1.1	4.9686	−0.63	4.994	−0.10
	100	5.055	1.1	4.9686	−0.63	4.994	−0.10
	2000	5.070	1.4	4.9686	−0.63	4.996	−0.06
	10,000	5.070	1.4	4.9686	−0.63	4.997	−0.06
13 (at E)	Solid	13.110	0.85	12.8184	−1.40	12.999	−0.01
	100	13.140	1.08	12.8184	−1.40	13.002	0.02
	2000	13.140	1.08	12.8331	−1.28	13.007	0.05
	10,000	13.170	1.31	12.8478	−1.17	13.007	0.06
24 (at IJ)	Solid	24.225	0.94	23.6817	−1.33	23.982	−0.07
	100	24.240	1.00	23.6964	−1.27	23.986	−0.05
	2000	24.270	1.13	23.7111	−1.20	23.969	−0.13
	10,000	24.315	1.31	23.7258	−1.14	23.971	−0.12

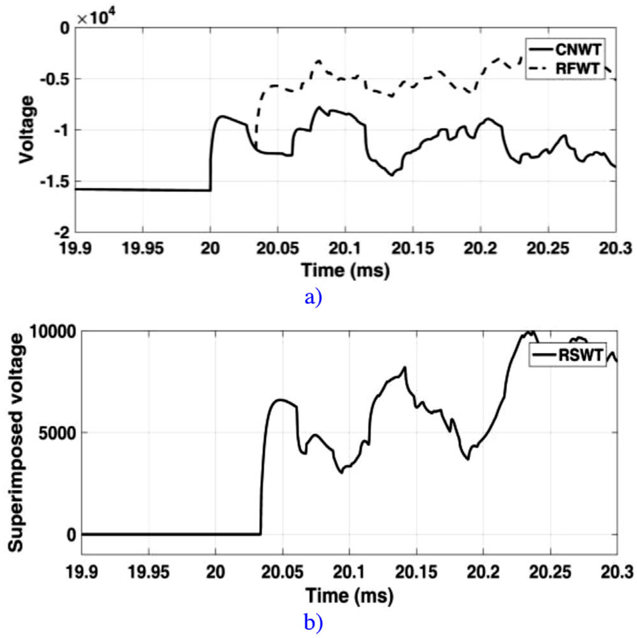

FIGURE 15 Response of [19] under earth fault F1 with unearthed distribution feeder illustrating the measured transient voltage. (a) Waveforms of closure-generating normal travelling waves (CNTW) and reclosure generating fault travelling wave (RFTW), (b) difference between the two cases

instant of the first difference (non-zero point). As depicted in Figure 14(c), the obtained time instants are 0.0337, 0.0874, and 0.1615 s under earth faults occurring at 5, 13, 24 km, respectively. Also, the response of this presented method in [15] was tested under significant fault resistances 100, 2000, 10,000 Ω as listed in Table 2.

The procedure presented in [19] was also implemented and tested under same fault cases as in Table 2 and Figure 15. Figure 15 illustrates in detail its response under the earth fault F1 associated with solid fault. Figure 15(a) shows both the transient voltage due to the circuit breaker closure-generating normal travelling waves (CNTW) and that due to the circuit breaker reclosure generating fault travelling waves (RFTW). Further, Figure 15(b) represents circuit breaker reclosure-generating superimposed travelling waves (RSWT) due to subtracting the two measured transient voltages depicted in Figure 15(a). As obtained from Figure 15(b), the first non-zero point is at 20.0338 s indicating to a fault at 4.9686 km distance. However, this method suffers from both the inaccurate control of the breaker reclosing angle and lack of applicability under the change of the network configuration before the fault occurrence. Also, as shown in Table 2, the proposed method is more accurate than the selected methods.

6.2 | Comparison with transient extraction methods

In the second phase of comparison, a comparative study between the proposed signal derivative procedure based on the adaptive threshold and other two surge extraction methods that are DWT [16] and Hilbert transform [23] is accomplished. The aim of the second stage is illustrating how that incorporating the proposed signal derivative procedure as transient extraction method in the proposed algorithm is the optimum solution. This is proved by comparing the obtained reflected surge arrival time and then the output of the fault-locator algorithm under different fault conditions. With respect to the DWT-based feature extraction, the Haar mother wavelet was found the most appropriate mother wavelet for extracting the stamping time of the arrival surge [16].

Owing to its smallest coefficient length, it provides a quick time tracking of the travelling surge better than the other mother wavelets. Its detail *d1* was found the most appropriate one to extract the arrival time stamp. Figure 16 shows the results of Haar mother wavelet for fault cases F1 and F2 with solid fault

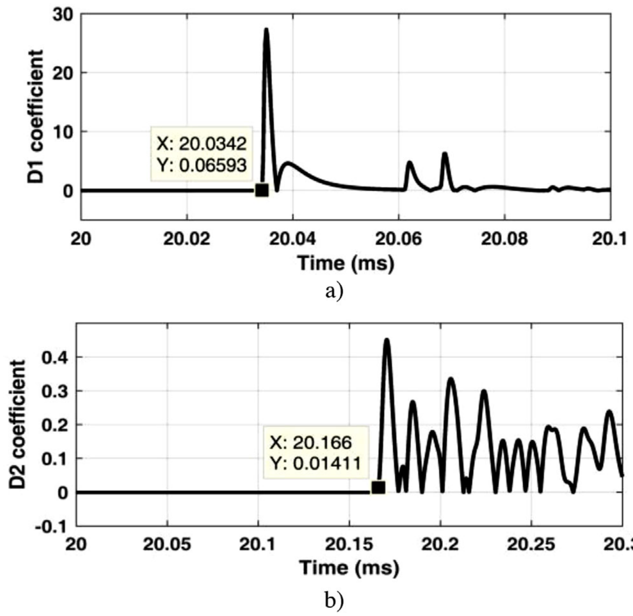

FIGURE 16 Reflected surge extraction with Haar wavelet (reclosing at 20 ms) under different fault conditions that are (a) fault case F1 at 5 km and (b) fault case F2 at 24 km

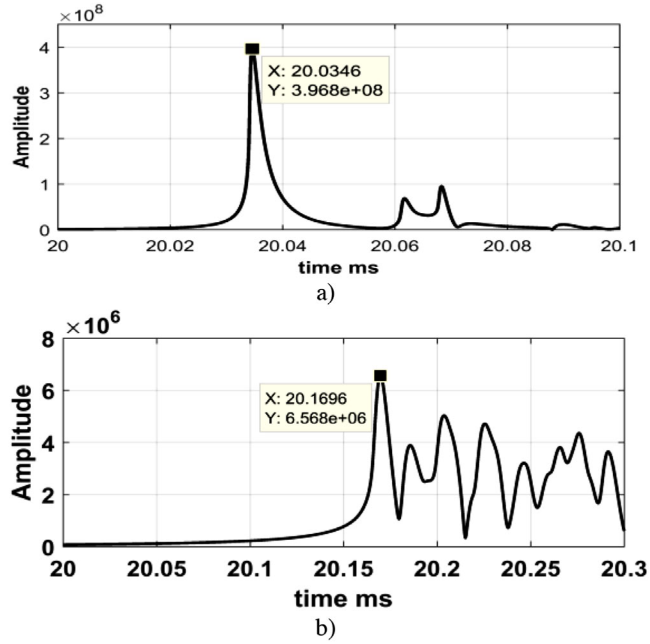

FIGURE 17 Reflected surge extraction with Hilbert transform (reclosing at 20 ms) under different fault conditions that are (a) fault case F1 at 5 km and (b) fault case F2 at 24 km

and a reclosing instant of 20 ms. A fixed threshold of 0.01 of the absolute value of the *d1* level gave the results as illustrated in Table 3 with errors of 0.548% and 1.67% for fault cases F1 and F2, respectively. Similarly, the corresponding error for the busbar fault at F3 was 0.846% as seen in Table 3. This ensures that the accuracy of the proposed algorithm and transient extraction using the Haar mother wavelet. However, longer fault distance produced higher error as seen in Table 3 due to the expected propagation attenuation. On the other hand, with respect to Hilbert–Haung transform, the detection of the high frequency sudden change points can be validated [23]. Also, the peak of Hilbert output can be used to obtain the arrival instant. However, the peak instant is not exactly at the arrival instant of the reflected surge from the fault point.

Figure 17 shows the response of Hilbert transform processed for the zero-mode voltage measured using the RC transducer. By stamping the peak of the Hilbert output, the time instants of 20.0346 and 20.1696 ms were realised at the peak for the fault cases F1 and F2 as seen in Figures 17(a) and (b), respectively. This resulted in fault location errors of 1.72% and 3.88% for both fault cases, respectively. These errors are still high as the Hilbert output first peak is matched with the highest frequency in the measured signal waveform, and it does not indicate the root instant of arrival surge. In other words, this highest frequency is expected at the front ramp time of the travelling surge instead of the surge root. The performance of Hilbert transform for time stamping with different fault resistances was evaluated as illustrated in Table 4. The Hilbert peak instant was fixed for each fault distance whatever the fault resistance up to 2 kΩ. This verified its capability for time stamping with both F1 and F2 fault cases with a wide fault resistance range. However, it has a higher fault location error of 3.88% for F2 fault case. Finally, Table 5 summarises the comparison study between the extraction methods along the selected range of the fault resistance in order to compare the three methods for extracting the arrival time of the reflected surges from the fault point. The results prove that the DWT was characterised by increasing error as higher fault resistance values increased for the far fault F2. Both Hilbert and signal derivative are not sensitive to the fault resistance, where the latter method (derivative-based technique) shows a better accuracy along the selected range of the fault distance. Accordingly, the signal derivative method with its tuned computation has the best performance for extracting the

TABLE 3 Haar mother wavelet for stamping the arrival time

Mother wavelet	Detail level	Stamped arrival time t_1 (ms)	Travelling time period $2t$ (ms)	Estimated fault distance d_e (km)	Error ε%
F1 at 5 km	d1	20.0342	0.0342	5.0274	0.548%
F2 at 24 km	d1	20.166	0.1660	24.402	1.67%
F3 at 13 km	d1	20.0892	0.0892	13.112	0.846%

TABLE 4 Effect of fault resistance on Hilbert transform-based time stamping

Fault Resistance R_f (Ω)	Fault case F1 (5 km) Peak value	Fault case F1 (5 km) Peak instant (ms)	Fault case F2 (24 km) Peak value	Fault case F2 (24 km) Peak instant (ms)
Solid	4.05E + 08	20.0346	6.69E + 06	20.1696
100	2.90E + 08	20.0346	4.90E + 06	20.1695
2000	4.56E + 07	20.0346	8.16E + 05	20.1693

TABLE 5 Comparison between discrete wavelet transform (DWT), Hilbert, and proposed derivative based on adaptive threshold

Fault case		DWT [16]		Hilbert [23]		Proposed derivative	
d_f	R_f (Ω)	d_e	ε%	d_e	ε%	d_e	ε%
5 km (section AB)	Solid	5.0274	0.548	5.086	1.724	4.994	–0.10
	100	5.0274	0.548	5.086	1.724	4.995	–0.08
	2000	5.0568	1.136	5.086	1.724	4.997	–0.04
13 km (busbar E)	Solid	13.112	0.864	13.033	0.257	13	0
	100	13.112	0.864	13.033	0.256	13.002	0.01
	2000	13.200	1.543	13.032	0.252	13.007	0.05
24 km (section IJ)	Solid	24.402	1.675	24.931	3.88	23.997	–0.01
	100	24.402	1.675	24.916	3.81	24.002	0.008
	2000	24.578	2.41	24.887	3.69	23.984	–0.06

reflected fault surges. Furthermore, it is the simplest one from the digital signal processing point of view. Therefore, it is the best extraction tool for realising the optimised fault distance estimation.

7 | CONCLUSIONS

A novel fault-locator algorithm for distribution networks has been presented based on the travelling waves created by triacs-based reclosing of the three phases of the faulted feeder. As the reflected surge has been mainly a function of the created surge through the faulted phase, the incident surge was increased by reclosing the triacs at the peak voltage of the faulted phase. Three methods have been used and compared to extract the arrival surge reflection from the fault point. These methods were theDWT, Hilbert transform, and the signal derivative approach. From the comparison tests, the signal derivative-based methodology was found the most accurate one. Extensive simulation tests corroborated the superior performance of the proposed method even with high resistive faults and different network configurations. This facilitates implementing a practical and versatile reclosing travelling-wave scheme for self-healing mechanisms in modern smart grids. Also, the performance of the proposed fault-locator algorithm has been compared with other two existed methods. The results have proved that the proposed method has been competitive to the two other methods from the accuracy point of view. Extending the presented algorithm to be independent of the feeder parameters is the main future prospective of such work to ensure better performance for aged distribution system.

REFERENCES

1. IEEE-PES Power System Relaying Committee: IEEE guide for determining fault location on ac transmission and distribution lines–C37.114-2014: Revision of IEEE Std C37.114-2004, pp. 1–76. IEEE, Piscataway (2015)
2. Nikander, A., Järventausta, P.: Identification of high-impedance earth faults in neutral isolated or compensated MV networks. IEEE Trans. Power Delivery 32(3), 1187–1195 (2017)
3. Kumpulainen, F.L., Kauhaniemi, K.: Review of methodologies for earth fault indication and location in compensated and unearthed MV distribution networks. In: Electric Power Systems Research, vol. 154, pp. 373–380. Elsevier, New York (2018)
4. Bo, Z.Q., et al.: Accurate fault location technique for distribution system using fault-generated high-frequency transient voltage signals. In: IEE Proceedings–Generation, Transmission & Distribution, vol. 146(1), pp. 73–79. IEEE, Piscataway (1999)
5. Elsadd, M.A., et al.: Earth fault location determination independent of fault impedance for distribution networks. In: International Transactions on Electrical Energy Systems, vol. 27(5), pp. 2389–2398. Wiley, Chichester (2017)
6. Elsadd, M.A., et al.: Incorporating earth fault location in management control scheme for distribution networks. In: IET Proceedings–Generation, Transmission & Distribution, vol. 10(10), 2389–2398. IEEE, Piscataway (2016)
7. Liang, R., et al.: Fault location based on single terminal travelling wave analysis in radial distribution network. Int. J. Electr. Power Energy Syst. 66, 160–165 (2015)
8. Lopes, F.V., et al.: Accurate two-terminal transmission line fault location using traveling waves. IEEE Trans. Power Delivery 33(2), 873–880 (2018)
9. Rui, L., et al.: Fault location for power grid based on transient travelling wave data fusion via asynchronous voltage measurements. In: International

Journal of Electrical Power & Energy Systems, 93, pp. 426–439. Elsevier Oxford (2017)
10. Nan, P., et al: Asynchronous fault location scheme for half-wavelength transmission lines based on propagation characteristics of voltage travelling waves. In: IET Proceedings–Generation, Transmission & Distribution, vol. 13(4), pp. 502–510. IEEE, Piscataway (2019)
11. Lopes, F.V., et al.: Practical methodology for two-terminal travelling wave-based fault location eliminating the need for line parameters and time synchronization. IEEE Trans. Power Delivery (2019). https://doi.org/10.1109/TPWRD.2019.2891538
12. Naidu, O.D., et al.: A travelling wave based fault location method using unsynchronized current measurements. IEEE Trans. Power Delivery 34(2), 505–513 (2019)
13. Hamidi, R.J., et al.: Traveling-wave-based fault-location algorithm for hybrid multiterminal circuits. IEEE Trans. Power Delivery 32(1), 135–144 (2017)
14. Lopes, F.V., et al.: Traveling wave-based solutions for transmission line two-terminal data time synchronization. IEEE Trans. Power Delivery 33(4), 3240–3241 (2018)
15. Zhou, C., et al.: A single-phase earth fault location scheme for distribution feeder on the basis of the difference of zero mode traveling waves. In: International Transactions on Electrical Energy Systems, vol. 27(5), Wiley, Chichester (2017)
16. Elkalashy, N.I., et al.: Earth fault distance estimation using travelling waves in energized compensated MV networks. IEEE Trans Power Delivery 30(2), 836–843 (2014)
17. Liang, R., et al.: Research of fault location in distribution networks based on integration of travelling wave time and frequency analysis. In: Proceedings of CSEE, 33, pp. 130–136. (2013). https://doi.org/10.13334/j.0258-8013.pcsee.2013.28.019
18. Hizam, H., Crossly, P.A.: Estimation of fault location on a radial distribution network using fault generated travelling waves signals. J. Appl. Sci. 7(23), 3737–3742 (2007)
19. Shi, S., et al.: Traveling waves-based fault location scheme for feeders in power distribution network. In: 14th International Conference on DPSP 2018, 23. IEEE, Piscataway (2018)
20. Gale, P., et al.: Fault location based on travelling wave. In: IEE 5th Conference on Developments in Power System Protection, York University, 30 March to 2 April 1993
21. Bo, Z.Q., et al.: Accurate fault location technique for distribution system using fault-generated high-frequency transient voltage signals. In: IET Proceedings–Generation, Transmission & Distribution, vol. 146(1), pp. 73–79. IEEE, Piscataway (1999)
22. Bo, Z.Q., et al.: Accurate fault location and protection scheme for power cable using fault generated high frequency voltage transients. In: Proceedings of 8th Mediterranean Electrotechnical Conference, Bari, Italy, vol. 2, pp. 777–780. IEEE, Piscataway (1996)
23. Elkalashy, N.I., et al.: Evaluation of chirp detector-based travelling wave localization of earth faults in MV networks. In: IET 10th DPSP 2010, Manchester, UK (2010)
24. Silva, M., et al.: A fault locator for transmission line using travelling wave and wavelet theory. In: 8th IEE International Conference on Developments in Power System Protection, Amsterdam, Netherlands, 5–8 April 2004
25. Lin, S., et al.: Travelling wave time–frequency characteristic-based fault location method for transmission lines. IET Gener. Transm. Distrib. 6(8), 764–772 (2012)
26. Chen, P., et al.: A travelling wave based fault locating system for HVDC transmission lines. In International Conference on Power System Technology, Chongqing, China, 22–26 October 2006
27. Gui-Bin, Z., Hou-lei, G.: Algorithm for ultra-high speed travelling wave protection with accurate fault location. In: 2008 IEEE Power and Energy Society General Meeting–Conversion and Delivery of Electrical Energy in the 21st Century, Pittsburgh, PA, USA, 20–24 July 2008
28. Zhang, J., et al.: Improving the accuracy of single-ended transient fault locator using mathematical morphology. In: International Conference on Power System Technology, Kunming, China, 13–17 October 2002
29. Xiao'an, Q., et al.: Traveling wave based distribution lines fault location using hilbert-huang transform. In: 2008 IEEE Industry Applications Society Annual Meeting, Edmonton, AB, Canada, 5–9 October 2008
30. Gale, P., et al.: Practical experience with travelling wave fault locators on Scottish power's 275 & 400 kV transmission system. In Proceedings of the Institution of Electrical Engineers–6th Conference on Developments in Power System Protection, Nottingham, U.K, pp. 192–196. IEEE, Piscataway (1997)
31. Tarhuni, N.G., et al.: Autonomous control strategy for fault management in distribution networks. In: Electric Power Systems Research, vol. 121(2), pp. 252–259. Elsevier, New York (2015)
32. Guzmán, G.S., et al.: Testing travelling-wave line protection and fault locators. In: 14th International Conference on Developments in Power System Protection (DPSP), IET, Belfast, UK (2018)
33. Sanseverino, E.R., et al.: A two-end travelling wave fault location system for MV Cables. IEEE Trans. Ind. Appl. 55(2), (2019)
34. Bashir, M.I., et al.: Considering characteristics of arc on travelling wave fault location algorithm for the transmission lines without using line parameters. In: TThe 10th International Conference on Environment and Electrical Engineering (EEEIC), Rome, Italy (2011)

How to cite this article: Elkalashy NI, Eldeeb HK, Kawady TA, Tarhuni NG, Lehtonen M, Taalab A-MI, Elsadd MA. Earth fault distance estimation using travelling waves provided with triacs-based reclosing in distribution networks. *IET Renew Power Gener.* 2021;15:43–57. https://doi.org/10.1049/rpg2.12004

APPENDIX: THE DATA OF THE TEST SYSTEM

The feeder parameters (positive- and zero-sequence resistance, inductance, and capacitance) are listed in Table A.1; whereas the lengths of the feeder's sections are listed in Table A.2. Also, the modelling system in the ATP-EMTP software is shown in Figure A.1.

TABLE A.1 Selected feeder parameters

Symbol	Quantity	Value	Unit
R_1	Positive sequence resistance	0.236087	(Ω km^{-1})
R_0	Zero sequence resistance	0.363293	(Ω km^{-1})
L_1	Positive sequence inductance	1.363074	(mH km^{-1})
L_0	Zero sequence inductance	5.268403	(mH km^{-1})
C_1	Positive sequence capacitance	0.021459	(μF km^{-1})
C_0	Zero sequence capacitance	0.012549	(μF km^{-1})

TABLE A.2 System data

Line No.	Terminals: Start Bus	Terminals: End Bus	Length
1	A	B	6
2	B	C	3
3	C	D	8
4	C	E	4
5	E	F	4
6	E	G	6
7	G	H	5
8	G	I	4
9	I	J	3
10	A	K	4
11	K	L	8
12	L	M	10
13	L	N	3
14	N	O	5
15	F	P	9
16	F	Q	5
17	K	R	7
18	N	S	9

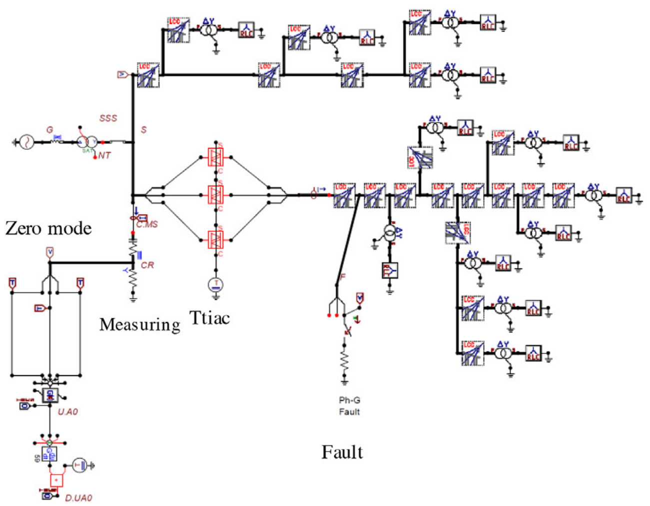

FIGURE A.1 ATPDraw circuit for the network feeders